Effect of Catalyst Distribution in a Membrane Reactor: Experiments and Model

John Szegner, King Lun Yeung, and Arvind Varma
Dept. of Chemical Engineering, University of Notre Dame, Notre Dame, IN 46556

Inorganic membrane reactors combine reaction and separation operations in a single unit. Preferential permeation of a product species through the membrane enhances equilibrium-limited reactions beyond the thermodynamic limit. Proper catalyst formulation and spatial distribution also enhance membrane reactor performance. To minimize reactant loss due to high gas permeation, the thickness of the γ-alumina layer in a composite alumina membrane (Membralox) was increased to 17 μm by slip-casting with alumina sol. Among the catalysts investigated, a formulation of 1.10 wt. % Pt and 1.36 wt. % Sn supported on γ-alumina pellets yielded the highest activity, selectivity, and stability for the dehydrogenation of ethane to ethylene. Using this catalyst composition, various nonuniform platinum distributions within the pellets were prepared by solution impregnation, while maintaining a uniform distribution of Sn. The effect of nonuniform catalyst distribution on dehydrogenation of ethane in a packed-bed membrane reactor (PBMR) under well-mixed, isothermal conditions was evaluated both experimentally and theoretically. Reactor performance is maximized when the catalyst is concentrated near the surface of the support. Supraequilibrium conversions, about 80% beyond equilibrium values, were obtained with the narrow surface-step catalyst pellets. Experimental results agree well with theoretical predictions, obtained without the use of any adjustable parameters. The effect of membrane thickness on reactor performance was also investigated, by comparing the 17- μm alumina membrane with a 1.2-mm-thick porous Vycor glass, using pellets with the narrow surface-step distribution. For the experimental conditions employed, relatively low permeation through the porous Vycor resulted in conversions near fixed-bed reactor values.

Introduction

Recent developments in the synthesis of inorganic membranes have led to high-temperature membrane reactor applications. Membrane reactors offer the advantage over conventional fixed-bed reactors (FBR) of combining separation and chemical reaction into a single unit. The membrane provides a medium for separation of product(s) formed within the pellets of a packed-bed membrane reactor (PBMR) or within the membrane of a catalytic membrane reactor (CMR). Significant improvements, above thermodynamic equilibrium values, can be achieved by selective removal of product(s) generated by equilibrium-limited reactions. Catalytic dehydrogenations are an example of this type, where product hydrogen is removed selectively. Improvements in product selectivity can also be realized by the preferential removal of reaction component(s) that have the potential to react further to form undesired product(s), as in the case of parallel-consecutive reactions (Bernstein and Lund, 1993). In other situations, improvements in reactor performance arise as a consequence of controlled reactant addition through the membrane. Examples include controlled addition of oxygen through the membrane in partial oxidation reactions of hydrocarbons (Santos et al., 1995; Tonkovich et al., 1996). Several articles, which review experimental and theoretical studies of catalytic membrane reactors, are available in the literature (c.f. Hsieh, 1991; Tsotsis et al., 1993; Saracco and Speccia, 1994; Zaman and Chakma, 1994).

Correspondence concerning this article should be addressed to A. Varma.
Current address of K. L. Yeung: Dept. of Chemical Engineering, Hong Kong University of Science and Technology, Clear Water Bay, Kowloon, Hong Kong.

In a combined experimental and theoretical study, Champagnie et al. (1992) studied the dehydrogenation of ethane, using a CMR configuration with a 5 wt. % platinum impregnated within the mesoporous layer of a cylindrical composite alumina membrane. This plug flow CMR was shown to exceed thermodynamic equilibrium values by the selective removal of hydrogen. Zaspalis et al. (1991) used a γ-alumina membrane in a PBMR configuration for the dehydrogenation of butane. Using a 6.2 wt. % Pt supported on SiO_2 as the catalyst resulted in the enhancement of conversion and selectivity by a factor of 1.5 and 1.6, respectively, as compared to a conventional fixed-bed reactor. Ziaka et al. (1993) investigated dehydrogenation of propane, with 5 wt. % Pt/γ-Al_2O_3 catalyst packed within the tube side of a Membralox composite γ-alumina membrane (thickness $\sim 1-5$ μm). This high-flux membrane resulted in propylene conversions 1.8 times higher than the corresponding equilibrium values. Porous Vycor (membrane thickness ~ 1.2 mm), which yields significantly lower flux values than the composite alumina, was studied for the dehydrogenation of cyclohexane to benzene in a well -mixed CMR (Sun and Khang, 1988). The platinum impregnated membrane exhibited considerable improvement in conversion, from 61% to 90%. However, to achieve this result, space times of 10 to 30 s (ca. 3.84 to 1.27 sccm inlet feed flow rates) were used, thus resulting in relatively small throughputs.

The performance of porous membrane reactors, which enhance reactor performance as a result of their ability to preferentially separate reaction product(s), is strongly dependent on the pore size, porosity, and thickness of the membrane. Recent advances in techniques such as slip casting and dip coating allow for precise control of the pore size and membrane thickness to achieve optimal permeation rates (Ward and Ko, 1995; Yeung et al., 1997). The effect of membrane thickness on reactor performance was evaluated theoretically, and it was shown that there exists an optimum membrane thickness that depends on the relative rates of permeation and reaction (Ito et al., 1985; Mohan and Govind, 1988).

While improvements in membrane design are possible, dehydrogenation reactions are frequently limited by catalyst activity rather than by the rate of hydrogen removal through the membrane (Raich and Foley, 1995). As a result, improved catalysts are desired. With supported metal catalysts for reactions involving paraffins, there are several metal catalyzed (e.g., dehydrogenation, isomerization, cyclization, aromatization, hydrogenolysis, and coking) and acid catalyzed (e.g., isomerization, cyclization, aromatization, hydrocracking, and coking) reactions possible (Beltramini and Trimm, 1987). Typically, dehydrogenation catalysts consist of Group VIII metals (mainly platinum) supported on oxide supports such as alumina or silica. In order to improve dehydrogenation selectivity, activity, and stability, promoters from Group VIII, VI, IB, or their combinations are often used (Sinfelt, 1983; Cavani and Trifiro, 1994). For dehydrogenation of a light paraffin such as ethane, using Pt without the addition of promoters results in relatively high hydrogenolysis activity to form methane. Tin is a commonly used promoter for light olefin dehydrogenation, resulting in improved catalyst selectivity and durability (Cavani and Trifiro, 1994; de Miguel et al., 1996).

Once the catalyst composition is established, further improvements in catalyst performance can be realized by proper spatial distribution of the active component within the support. The idea of distributing the catalyst nonuniformly in pellets has been studied extensively. Some general results have been obtained for the typical case where the catalyst loading is not high, so that the catalyst surface area increases linearly with loading. For this case, using the variational method it was demonstrated that for catalyst performance indexes such as effectiveness, selectivity, or yield, and for the most general case of an arbitrary number of reactions, with arbitrary kinetics, occurring in a nonisothermal pellet, with finite external mass and heat-transfer resistances, the optimal distribution is a step function. For higher loadings, where the catalyst surface area increases nonlinearly with loading, the optimal catalyst distribution in general must be determined numerically (Baratti et al., 1993). The area of optimal distribution of catalyst in pellets, including both theoretical and experimental developments, has been reviewed recently by Gavriilidis et al. (1993).

The concept of nonuniform catalyst distribution within the pellets of a PBMR, well-mixed on both the feed and permeate sides, has also been demonstrated recently. It has been shown theoretically that for many cases of practical interest, optimal PBMR performance can be achieved by distributing the catalyst as a step function within the pellets (Yeung et al., 1994). Experimentally, Cannon and Hacskaylo (1992) studied cyclohexane dehydrogenation in inert and active porous Vycor glass tubes packed with Pd/Al_2O_3 catalyst granules. Superior reactor performance was achieved for the case where Pd was deposited on both the inner and outer surfaces of the tube. More recently, Yeung et al. (1996) have shown improved performance of Pd-composite membrane reactors for ethane dehydrogenation using a nonuniform distribution (narrow surface-step) of Pt-Sn/γ-alumina catalyst.

In the preceding examples involving membrane reactors, the enhancement in reactor performance was obtained as a result of preferential product separation through the porous membrane. However, further improvement in reactor performance can be achieved by proper catalyst selection, optimal spatial distribution of the active component within the support, and by choosing a suitable membrane thickness to reduce reactant losses. In this article, we address these issues for the dehydrogenation of ethane in a well-mixed PBMR. First, we systematically investigate several Pt-Sn/γ-alumina mixtures, to determine the catalyst composition that yields the best performance. Next, the effect of varying catalyst activity distribution within the porous pellets on a PBMR performance is demonstrated quantitatively, using both experiments and model, with a sol-gel slip-cast-modified composite alumina membrane. Finally, the effect of membrane thickness on reactor performance is also examined.

Theoretical Model

As noted earlier, the optimal distribution of catalyst within the pellets of a well-mixed PBMR is a step function. To demonstrate the effect of nonuniform catalyst distribution, a model was developed and tested numerically using dehydrogenation of ethane as an example. The well-mixed PBMR (obtained using high recycle ratio) is shown in Figure 1, where the reaction mixture is introduced on the tube side of the

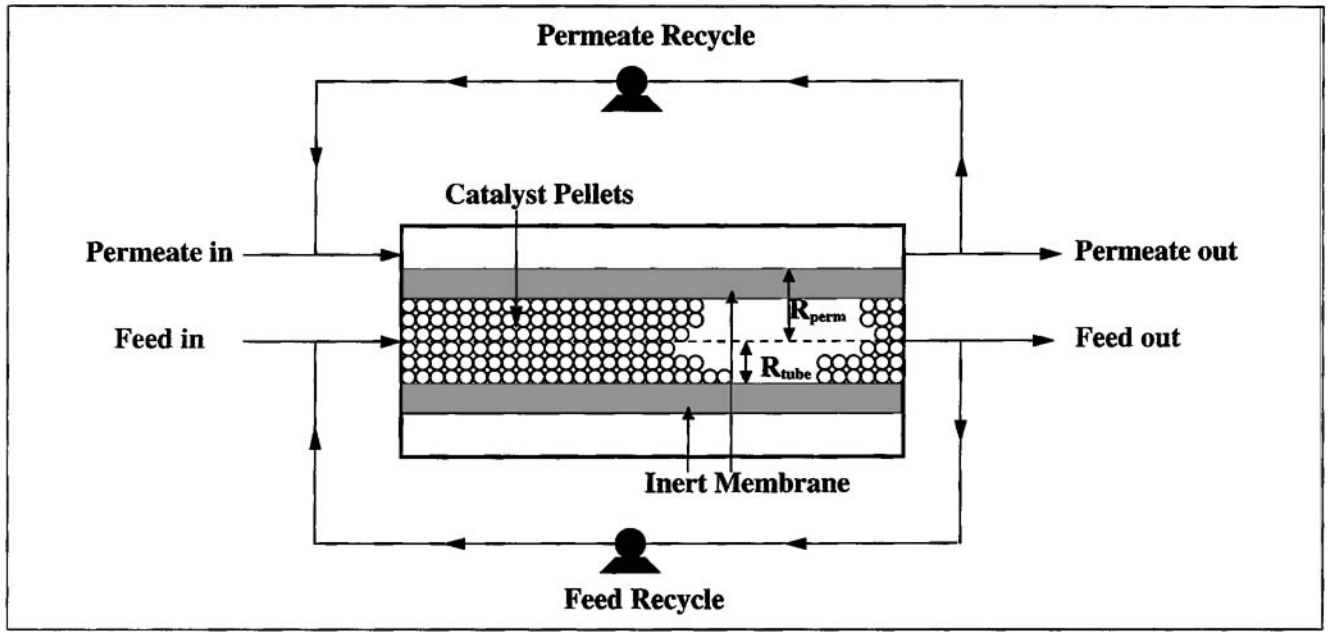

Figure 1. PBMR with recycle streams.

membrane packed with catalyst pellets. On the permeate side, an inert sweep gas is introduced to remove the components that permeate through the inert membrane.

The model is based on the following assumptions.

- Isothermal and steady-state conditions
- Well-mixed conditions on both the tube and permeate sides
- Negligible mass-transfer resistance between the bulk gas and external surface of both the membrane and the pellets
- Negligible pressure drop on both the tube and permeate sides
- Constant feed molar flow rates and compositions
- Constant effective diffusivities in both the membrane and the pellets
- Negligible axial and radial dispersion on both the tube and permeate sides.

In accordance with these assumptions, the model equations are developed for the dehydrogenation of ethane:

$$C_2H_6 \Leftrightarrow C_2H_4 + H_2, \tag{1}$$

where i refers to a reaction component (i.e., C_2H_6, C_2H_4, H_2, and the inert Ar).

The mass balance on the tube side of the membrane is given by

$$Q^o_{\text{tube}} x_i^o - Q_{\text{tube}} x_i + \frac{2\pi L D_{mi}}{R_G T}\left[r_m \frac{dp_{mi}}{dr_m}\right]_{r_m = R_{\text{tube}}} + \nu_i V_{\text{cat}} \tilde{R}(p_{pi}) = 0, \tag{2}$$

where ν_i is the stoichiometric coefficient, -1 for the reactant (C_2H_6), $+1$ for the products (C_2H_4 and H_2), and zero for the inert Ar.

On the permeate side, we have

$$Q^o_{\text{perm}} y_i^o - Q_{\text{perm}} y_i - \frac{2\pi L D_{mi}}{R_G T}\left[r_m \frac{dp_{mi}}{dr_m}\right]_{r_m = R_{\text{perm}}} = 0. \tag{3}$$

In the inert membrane, the mass balance yields

$$\frac{D_{mi}}{R_G T}\frac{1}{r_m}\frac{d}{dr_m}\left[r_m \frac{dp_{mi}}{dr_m}\right] = 0; \qquad R_{\text{tube}} \le r_m \le R_{\text{perm}} \tag{4}$$

along with the boundary conditions (BCs)

$$p_{mi} = x_i P_{\text{tube}} \quad @\ r_m = R_{\text{tube}} \tag{5a}$$

$$p_{mi} = y_i P_{\text{perm}} \quad @\ r_m = R_{\text{perm}}. \tag{5b}$$

The term $\tilde{R}(p_{pi})$ appearing in Eq. 2 represents the reaction rate per unit solid volume, given by

$$\tilde{R}(p_{pi}) = \frac{1}{V_p}\int_{V_p} k S_A \left[p_{pC_2H_6} - \frac{p_{pC_2H_4} p_{pH_2}}{K_{eq}}\right] dV_p, \tag{6}$$

where S_A is defined as the active surface area per unit catalyst volume, given by

$$S_A = \frac{a \rho_c C_e}{1 + bC_e}, \tag{7}$$

where C_e represents the catalyst loading (weight of active element/weight of catalyst pellet); a is the specific surface area of active element (i.e., active element surface area/active element weight); ρ_c is pellet density; and b is a constant (cata-

lyst pellet weight/active element weight) that is responsible for the deviation from linear behavior.

The preceding equations are coupled with the steady-state mass balance for spherical catalyst pellets

$$\frac{D_{pi}}{R_G T}\frac{1}{r_p^2}\frac{d}{dr_p^2}\left[r_p^2\frac{dp_{pi}}{dr_p^2}\right] = -\nu_i k a \rho_c \bar{C}_e \frac{\mu(w)}{1+B\mu(w)}\left[p_{pC_2H_6} - \frac{p_{pC_2H_4}p_{pH_2}}{K_{eq}}\right], \quad (8)$$

along with the BCs

$$\frac{dp_{pi}}{dr_p} = 0 \qquad @\ r_p = 0 \quad (9a)$$

$$p_{pi} = x_i P_{\text{tube}} \qquad @\ r_p = R_p. \quad (9b)$$

Introducing the dimensionless quantities:

$$u_i = \frac{p_{mi}}{P_{\text{tube}}}, \quad \psi_i = \frac{p_{pi}}{P_{\text{tube}}}, \quad w = \frac{r_p}{R_p}, \quad s = \frac{\ln\left(\frac{r_m}{R_{\text{tube}}}\right)}{\delta},$$

$$\delta = \ln\left(\frac{R_{\text{perm}}}{R_{\text{tube}}}\right), \quad P_r = \frac{P_{\text{perm}}}{P_{\text{tube}}}, \quad \mu = \frac{C_e}{\bar{C}_e}, \quad B = b\bar{C}_e$$

$$\beta_{\text{tube}} = \frac{Q_{\text{tube}}}{Q^o_{\text{tube}}}, \quad \beta_{\text{perm}} = \frac{Q_{\text{perm}}}{Q^o_{\text{tube}}}, \quad \beta^o_{\text{perm}} = \frac{Q^o_{\text{perm}}}{Q^o_{\text{tube}}},$$

$$\alpha_{mi} = \frac{D_{mi}}{D_{mC_2H_6}}, \quad \alpha_{pi} = \frac{D_{pi}}{D_{pC_2H_6}}, \quad K_{eq} = \frac{K}{P_{\text{tube}}},$$

$$\phi_p = R_p\sqrt{\frac{R_G T k a \rho_c \bar{C}_e}{D_{pC_2H_6}}}, \quad \theta = \frac{2\pi D_{mC_2H_6} P_{\text{tube}} L}{R_G T Q^o_{\text{tube}}},$$

$$\varphi = \frac{3 D_{pC_2H_6} P_{\text{tube}} L V_{\text{cat}}}{R_G T Q^o_{\text{tube}} R_p^2}. \quad (10)$$

Equations 2 to 9 can be reduced to dimensionless forms. Since the membrane is inert, Eq. 4 along with the corresponding BCs can be solved analytically, to give

$$u_i(s) = (y_i P_r - x_i)s + x_i; \qquad 0 \le s \le 1. \quad (11)$$

Within the pellets, the mass balance takes the dimensionless form

$$\frac{1}{w^2}\frac{d}{dw}\left[w^2\frac{d\psi_i}{dw}\right] = -\frac{\nu_i}{\alpha_{pi}}\phi_p^2\frac{\mu(w)}{1+B\mu(w)}\left[\psi_{C_2H_6} - \frac{\psi_{C_2H_4}\psi_{H_2}}{K_{eq}}\right], \quad (12)$$

along with the BCs

$$\frac{d\psi_i}{dw} = 0 \qquad @\ w = 0 \quad (13a)$$

$$\psi_i = x_i \qquad @\ w = 1. \quad (13b)$$

On the tube side, we have

$$x_i^o - \beta_{\text{tube}} x_i + \frac{\theta\alpha_{mi}}{\delta}\left[\frac{du_i}{ds}\right]_{s=0} - \varphi\alpha_{pi}\left[\frac{d\psi_i}{dw}\right]_{w=1} = 0, \quad (14)$$

where the last term represents the flux at the pellet surface, and arises from substituting the pellet Eq. 8 into Eq. 6 and integrating by parts.

On the permeate side, we obtain

$$\beta^o_{\text{perm}} y_i^o - \beta_{\text{perm}} y_i - \frac{\theta\alpha_{mi}}{\delta}\left[\frac{du_i}{ds}\right]_{s=1} = 0, \quad (15)$$

while the definition of the activity distribution function, $\mu(w)$ leads to the constraint

$$\int_0^1 \mu(w) w^2\, dw = \frac{1}{3}. \quad (16)$$

The solution of Eqs. 11–16, coupled with the congruence conditions

$$\Sigma_i x_i = 1 \quad \text{and} \quad \Sigma_i y_i = 1, \quad (17)$$

provide the dimensionless molar flow rates β_{tube} and β_{perm}, the mole fractions x_i and y_i, and the concentration profiles within the pellets ψ_i.

Four step-type catalyst distributions with varying active layer thicknesses and locations (preparation and characterization discussed in the Experimental section) as shown in Figures 2a to 2d, were studied, and their characteristics are summarized in Table 1. For the various distributions, $\mu(w)$ was determined using Eq. 16.

The pellet equations were solved using orthogonal collocation on finite elements (Villadsen and Michelsen, 1978; Finlayson, 1980), and the resulting nonlinear algebraic equations were solved numerically using the IMSL subroutine DNEQNF (IMSL, 1989). Mass balance equations for the inert regions were solved analytically, and coupled with equations for the active layer through the BCs, assuming continuity of concentrations and flux.

Experimental Studies

Various experimental techniques and apparatus used in the present work are described in this section. The composite alumina membrane was prepared using a sequential slip-casting technique. For the catalyst pellets, solution and sequential impregnation techniques were used to prepare catalysts with nonuniform activity distributions. The catalysts were characterized using hydrogen chemisorption and energy dispersive X-ray spectroscopy. An automated experimental setup used for both permeation and reaction studies was designed and constructed.

Membrane preparation and characterization

A composite alumina membrane (Membralox, US Filter) was modified by sequential slip casting of alumina sol. The original Membralox tube (25.0-cm length, 0.7-cm I.D., and

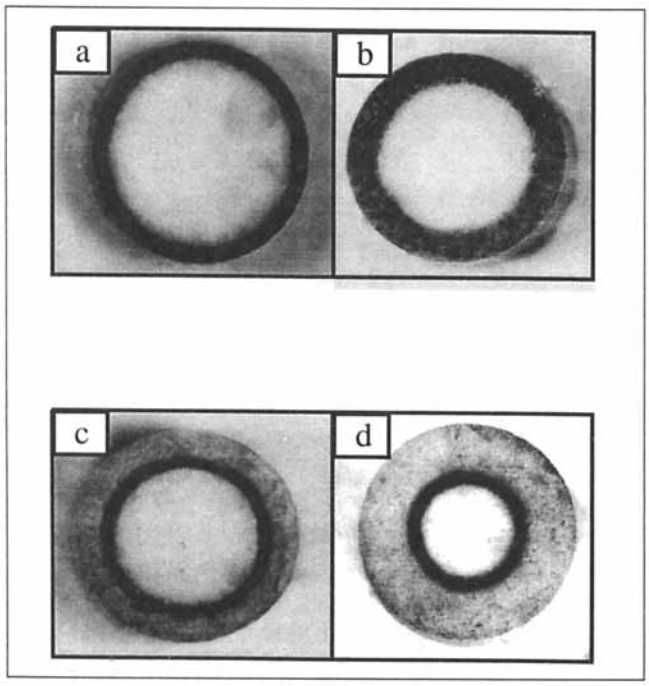

Figure 2. Pt-Sn/γ-Al_2O_3 pellets with different platinum distributions.

(a) Narrow surface-step, 0.0159 M hexachloroplatinic acid (15 min); (b) wide surface-step, 0.0121 M hexachloroplatinic acid (15 h); (c) near surface-step, sequential impregnation of 0.020 M hexachloroplatinic acid (15 min), and 0.0825 M citric acid (15 min); and (d) deep subsurface-step, sequential impregnation of 0.020 M hexachloroplatinic acid (30 min), and 0.0825 M citric acid (45 min).

1.0-cm O.D.) consisted of multiple layers: a 2-μm-thick γ-alumina (5-nm pore size), 30 μm of intermediate aluminas (0.2 μm pores), deposited on a ~1.5-mm macroporous (10 μm pores) α-alumina support. The γ-alumina membrane thickness was increased by slip casting the alumina sol layer by layer.

The sol used for the slip casting was a commercially available solution containing suspension of 50-nm colloidal boehmite particles (Dispal 23N4-20, Vista Chemical Company). The sol, which initially contained 20 wt. % alumina, was diluted using deionized distilled water to 5 wt. %. To minimize the formation of cracks and defects during the drying process, the diluted sol was modified by the addition of a binder, 5 wt. % polyvinyl alcohol (PVA, MW = 85,000 to 146,000) (Yeung et al., 1997). Prior to slip-casting, the sol was sonified for 10 min to minimize the agglomeration of particles in the suspension. The tube side of the Membralox membrane was contacted with the PVA containing alumina sol for a slip-cast time of 10 s.

Subsequent to slip casting, a careful drying procedure was employed to further decrease the formation of cracks and defects. The slip-cast boehmite film was dried for 12 h under a humid (~60% relative humidity) stream of air that was passed through the tube side of the membrane, while the outer macroporous α-alumina portion of the support was contacted with ambient air. This allowed the high-moisture-containing deposited alumina layer to dry at a slower rate, thus minimizing stress accumulation, which can lead to crack formation (Uhlhorn et al., 1992; Yeung et al., 1997). Following humid drying, the slip-cast membrane was dried in ambient air for 12 h.

The γ-alumina was obtained by calcining the slip-cast boehmite in 100 sccm stream of air following the procedure: ramp to 200°C in 2 h, hold for 3 h, ramp to 600°C in 6 h, hold for 12 h, and finally cool to room temperature. The slip-casting, drying, and calcining steps were repeated until the desired permeation flux was obtained. The membrane thickness was obtained from measurements of micrographs using a scanning electron microscope (SEM, ISI 60).

The pore size and specific surface area of the deposited layers were obtained by BET measurements, using the γ-alumina derived from the unsupported sol dried in a petri dish, and calcined using the same conditions as described before. The BET measurements were obtained using an AUTOSORB-1 (Quantachrome Corporation) physisorption unit where the analysis was based on the static volumetric method. The carrier (He) and adsorbing (N_2) gases were ultrahigh-purity grade. Prior to analysis, the samples were outgassed at 300°C.

Catalyst preparation

Impregnation with Platinum. The platinum step-type distributions were obtained by solution and sequential impregnation techniques using hexachloroplatinic acid and citric acid. The aqueous solutions of acids were prepared by adding dihydrogen hexachloroplatinate (IV) (Aldrich, A.C.S. grade) and citric acid (Fisher Scientific, A.C.S. grade) to deionized water. Prior to the impregnation steps, the γ-Al_2O_3 pellets (Engelhard, AL-3438 T, 3-mm right-cylindrical pellets) were calcined at 750°C for 3 h, then stored in air at 125°C. The pore diameter and specific surface area of the pellets were 9.7 nm and 168 m^2/g, respectively, as determined by BET measurements.

The solution impregnation technique involved contacting the γ-Al_2O_3 pellets (about 4 g) with hexachloroplatinic acid (20 mL) for a given length of time. For the sequential impregnation procedure, the pellets were contacted with hexachloroplatinic acid (20 mL) and citric acid (20 mL), consecutively, for desired impregnation times. Additional details

Table 1. Characteristics of Nonuniform Catalyst Pellets

Catalyst Distribution	Active Layer Center (R_c/R_p)	Active Layer Width (Δ/R_p)	Pt Loading (wt. %)	Sn Loading (wt. %)	Pt Dispersion (Pt/γ-Al_2O_3)	Pt Dispersion (Pt-Sn/γ-Al_2O_3)
Narrow surface-step	0.95	~0.10	1.11	1.36	64.7%	61.5%
Wide surface-step	0.875	~0.25	1.17	1.43	57.8%	60.4%
Near surface-step	0.70	~0.10	1.09	1.34	43.2%	42.2%
Deep subsurface-step	0.50	~0.10	1.16	1.35	34.8%	35.7%

Table 2. Heat-treatment Procedure for Pt and Pt-Sn Catalysts

Heat Treatment for Pt Catalyst				Heat Treatment for Pt-Sn Catalyst			
Temp. Ramp or Hold	Ramp or Hold Time	Gas	Gas Flow Rate	Temp. Ramp or Hold	Ramp or Hold Time	Gas	Gas Flow Rate
Room to 120°C	5 min	Ar	50 std. cm^3	Room to 120°C	30 min	Ar/O_2	100 std. cm^3
120°C	2 h	Ar	50 std. cm^3	120°C	4 h	Ar/O_2	100 std. cm^3
120°C to 550°C	2 h	O_2	50 std. cm^3	120°C to 300°C	30 min	O_2	50 std. cm^3
550°C	15 min	Ar	50 std. cm^3	300°C	2 h	O_2	50 std. cm^3
550°C	6 h	H_2	50 std. cm^3	300°C to 550°C	30 min	H_2	50 std. cm^3
550°C to room	3 h	Ar	50 std. cm^3	550°C	2 h	H_2	50 std. cm^3
				550°C to room	3 h	Ar	50 std. cm^3

about the impregnation techniques are given elsewhere (Papageorgiou et al., 1996).

The catalyst pellets with the various nonuniform platinum distributions are shown is Figures 2a to 2d. The platinum loadings were determined by flame atomic absorption spectrometry (SpectrAA-20, Varian), using the hexachloroplatinic acid solutions before and after impregnation. The narrow surface-step (Figure 2a) and the wide surface-step (Figure 2b) platinum distributions were obtained by impregnating the γ-Al_2O_3 pellets for different times in solutions containing hexachloroplatinic acid only. The near surface-step (Figure 2c) and deep subsurface-step (Figure 2d) platinum distributions were obtained by sequential impregnation. The function of the citric acid in these cases was to displace the $PtCl_6^{-2}$ anions and push them deeper within the γ-Al_2O_3 support (Lee and Aris, 1985; Papageorgiou et al., 1996). After impregnation, the catalysts were dried in air at 75°C for 12 h, followed by oxidation and reduction steps using the conditions shown in Table 2.

Impregnation with Tin. After preparation of the Pt/γ-Al_2O_3 catalyst as just described, tin was added by evaporative impregnation of tributyltinacetate dissolved in a 20-mL solution of *n*-pentane (Cortright and Dumesic, 1994). By partially covering the beaker containing the catalyst and the impregnation solution, complete evaporation time was maintained at ~ 5 h. After impregnation, the catalyst was kept at ambient conditions for ~ 12 h, followed by calcining using the procedure shown in Table 2 (Cortright and Dumesic, 1994).

Unlike Pt/γ-Al_2O_3 which turned from dark gray to black (see Figures 2a to 2d) upon reduction in hydrogen, the supported tin remained undetectable to visual observation. Hence the distribution of tin was determined qualitatively using energy-dispersive X-ray spectroscopy (EDXS) (Huang et al., 1996). A scanning electron microscope (ISI 60) along with an EDXS system (Microtrace Silicon X-ray Spectrometer, Moran Industries Inc.) equipped with a beryllium window and a Si(Li) detector was used to scan the radial positions within the pellets.

Chemisorption

The accessibility of platinum atoms, for both Pt and Pt-Sn catalysts supported on γ-Al_2O_3, was determined by dynamic pulsed chemisorption of hydrogen (Freel, 1972; Sarkany and Gonzalez, 1982). Prior to the chemisorption experiments, the samples were reduced using ultrahigh-purity hydrogen (50 std. cm^3) for 2 h and then purged in a stream of ultrahigh-purity argon (150 std. cm^3) for 4 h at 300°C. The sample was cooled to room temperature in 150 std. cm^3 flowing Ar before pulsing pure hydrogen. The hydrogen pulse size was 50 μL and the time between the pulses was 3 min. The experiments for each sample were repeated several times, to ensure reproducibility, which was within $\pm 5\%$.

Apparatus for reaction studies

The performance of a PBMR for the different catalyst distributions was evaluated for the dehydrogenation of ethane to ethylene using the experimental setup depicted in Figure 3. The catalyst pellets were packed within the tube side of the membrane, which was sealed to a stainless-steel casing by wrapping graphite strings around the ends of the tube. The reactant gas mixture (ethane, hydrogen, and argon) was introduced into the tube side, while pure argon was fed on the permeate side as sweep gas. The gas flow rates, on the feed and permeate sides, were controlled using UFC 1100A (Unit Instruments) mass-flow controllers. The feed-side pressure was monitored and controlled using a BROOKS 5866 (Brooks Instruments) pressure transducer and controller. Both sides were maintained under well-mixed conditions by using diaphragm pumps with gas recycle ratios of ~ 170. The reaction unit consisted of preheaters on both feed and permeate sides, which were not only used to preheat the reaction gases but also to promote the mixing of the recycle streams with the fresh feeds on both sides. The gases were then delivered to the furnace containing three zones, which allowed for uniform axial temperature distribution within the reactor. The temperatures were controlled to within ± 2°C using a Labview (Version 3.01, National Instruments) program containing five independent PID controllers.

The feed and permeate exit streams were analyzed using a Hewlett-Packard 5890 Series II gas chromatograph equipped with a TCD and FID connected in series. The sampling of the feed and permeate streams was performed using an air-actuated 10-way valve (Valco Instruments Co., Inc.). A 100/120-mesh Hayesep D packed column [20 ft (6.1 m)] was employed for the analysis of ethane, ethylene, and methane. The peak integration was performed by the Labview program.

The same apparatus was also used for membrane permeation measurements. These measurements were made at 525°C, for varying tube-side pressures, in the absence of sweep gas. The permeating gas flow rate was measured at ambient conditions using a bubble flowmeter.

Reaction conditions

For the membrane reactor experiments, a total of 3.1 g catalyst was used. The feed side was maintained at 0.6 psig,

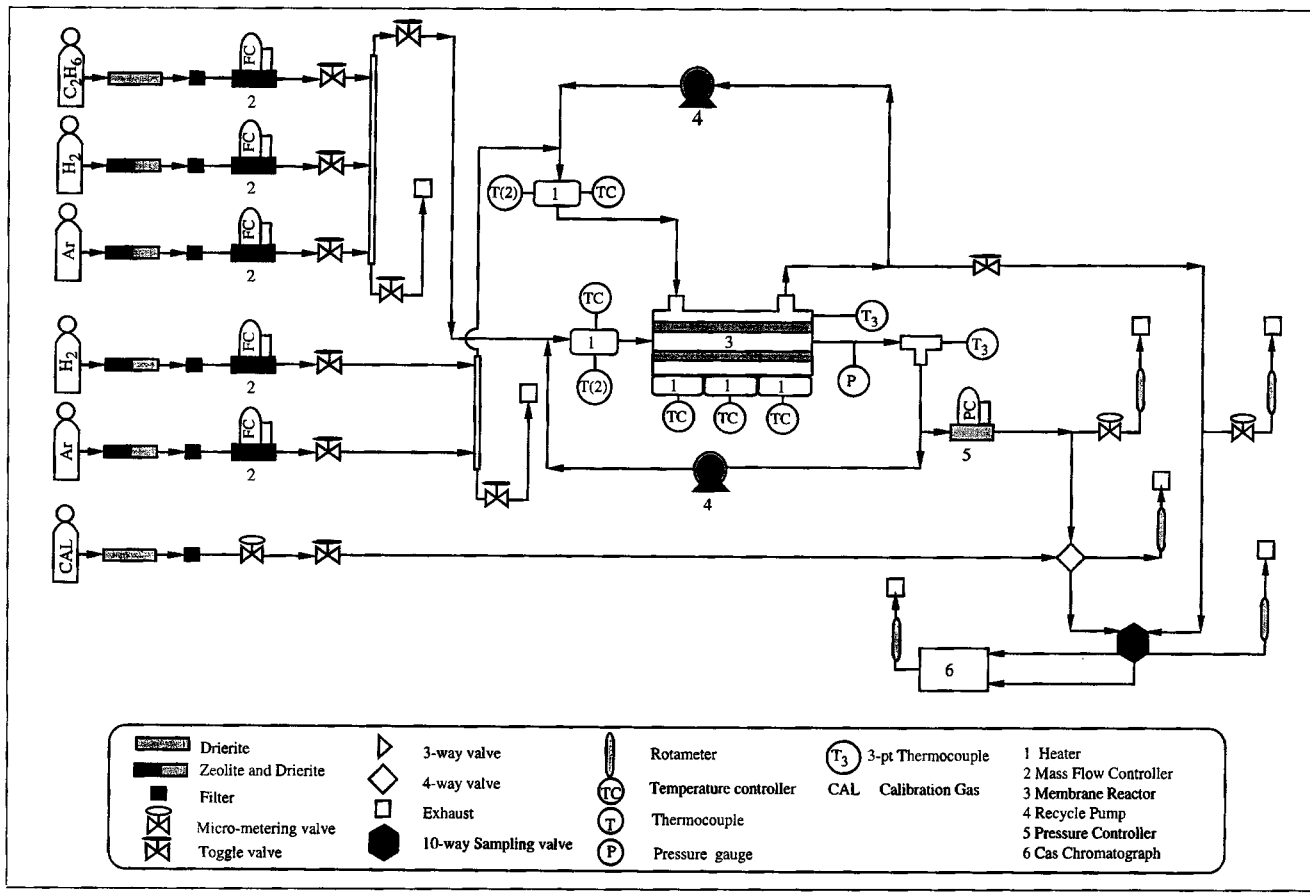

Figure 3. Experimental setup for the PBMR.

while the permeate side was kept at atmospheric pressure. With the exception of the experiments where the effect of reactant concentrations was studied, the fresh feed composition was maintained fixed at 10 mol % ethane (50% ethane/Ar mixture), 5 mol % hydrogen (HP grade), and balance argon (HP grade). The sweep ratio, defined as the ratio of the initial permeate and feed molar flow rates (Q^o_{perm}/Q^o_{tube}) was maintained at unity for all experiments, except for those where the effect of this ratio was studied. When the residence time (W_{cat}/Q^o_{tube}) was varied the temperature was kept fixed at 525°C, while for varying reactor temperatures, the residence time (W_{cat}/Q^o_{tube}) was maintained at 0.2×10^{-5} g catal·s/mol (feed flow rate of 200 std. cm^3).

For the catalyst selection and intrinsic kinetic experiments, the membrane reactor (shown in Figure 3) was replaced by a fixed-bed reactor (FBR) that consisted of a stainless-steel (304-SS) tube packed with Pt-Sn/γ-Al_2O_3 catalysts. These experiments were also carried out under well-mixed conditions, with the catalyst packed within the stainless-steel tube in the form of pellets (catalyst selection experiments) or powder (intrinsic kinetic studies). For the catalyst selection experiments, the temperature and pressure were maintained at 550°C and 4 psig, respectively, and the feed composition was kept fixed at 20% ethane, 5% hydrogen, and balance argon. For the intrinsic kinetic studies, the pressure was kept at 0.6 psig while the reaction temperature, ethane feed concentrations, and residence times were varied.

From all reaction studies, the activation procedure involved heating the catalyst in a 10% H_2/Ar mixture to the reaction temperature at a rate of 1.5°C/min. At this temperature, the reaction mixture was introduced and was maintained for 2 h to ensure steady state before commencing analysis. Reactor conversions were calculated based on the total moles of ethylene produced and measured at the exit of both the feed and permeate sides of the reactor, per mole of ethane introduced into the fresh feed.

Results and Discussion

Membrane permeation

To minimize reactant loss, the effective permeation rates were reduced by increasing the γ-Al_2O_3 membrane thickness of the original Membralox tube, with the slip casting of alumina sol. The micrographs of the original and slip-cast-modified membranes are shown in Figures 4a and 4b, respectively. Figure 4b depicts two distinct slip-cast $\sim$7-μm γ-Al_2O_3 layers, deposited on top of the original $\sim$2-μm membrane. These layers were found to be free of cracks and defects. The BET measurements of the average pore diameter and specific surface area of the deposited layers were 7.0 nm and 225 m^2/g, respectively.

Figures 5a and 5b show the argon and hydrogen permeation fluxes and separation factors corresponding to the original ($\sim$2 μm thick) and slip-cast-modified ($\sim$17 μm thick) membranes. With the addition of the $\sim$15-μm γ-Al_2O_3 layer, the argon permeation flux was reduced by nearly threefold.

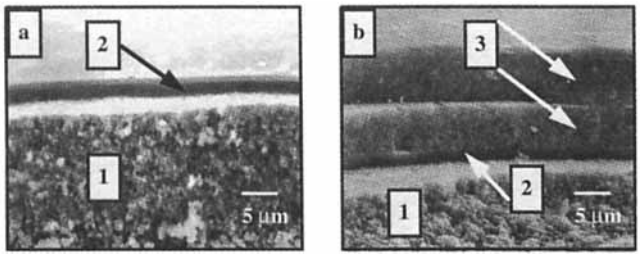

Figure 4. SEM micrograph: (a) original Membralox and (b) slip-cast modified Membralox tubular membrane.

(1) Intermediate alumina; (2) original γ-alumina (Membralox); and (3) slip-cast γ-alumina.

Also, Figure 5b indicates that the predominant diffusion mechanism is in the Knudsen regime, and that the addition of the slip-cast layers results in a slight improvement toward the ideal Knudsen value of 4.47. Based on the permeation measurements, the effective diffusivities of argon and hydrogen were 5.03×10^{-3} and 2.31×10^{-2} cm^2/s, respectively. The corresponding ideal Knudsen diffusivities for argon and hydrogen, based on the measured pore size and porosity, were calculated to be 5.44×10^{-3} and 2.43×10^{-2} cm^2/s, respectively.

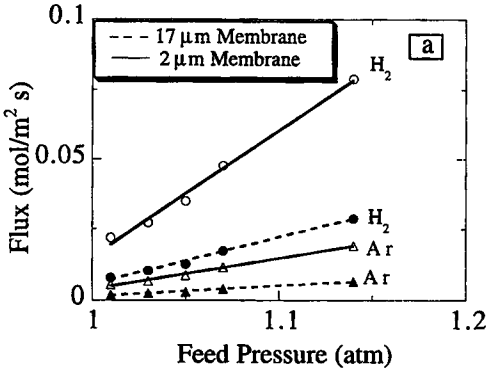

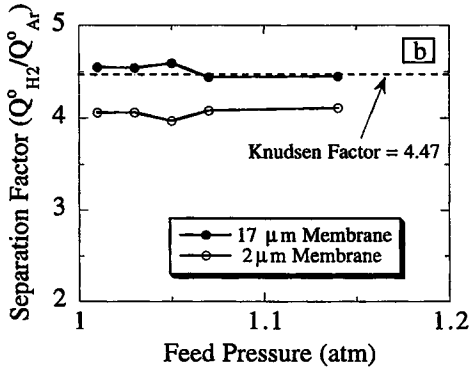

Figure 5. Hydrogen and argon (a) permeation rates, and (b) separation factor as a function of feed-side pressure.

The original (~ 2-μm γ-alumina) and the slip-cast modified (~ 17-μm γ-alumina) Membralox membranes at 525°C.

The permeation fluxes of argon and hydrogen were also measured for a porous Vycor glass tube (25.0 cm in length, with 0.76 and 1.0 cm inner and outer diameters, respectively) with an average pore diameter of 4.6 nm. Unlike the composite alumina membrane where the actual membrane layer thickness was only a few microns, however, the porous Vycor had a much larger membrane thickness of ~ 1.2 mm. As a result, the argon and hydrogen permeation values were measured to be ~ 170 times smaller than those for the slip-cast-modified composite alumina (~ 17-μm) membrane.

Catalyst selection

The Pt-Sn/γ-Al_2O_3 catalyst was chosen for the dehydrogenation of ethane to ethylene, where the competing reactions are coking and hydrogenolysis to form methane. In order to determine the best catalyst composition to yield the highest ethane dehydrogenation activity and selectivity, with the minimum amount of deactivation, platinum and tin in varying amounts and ratios were examined.

Figures 6a to 6d depict the conversion and selectivity as a function of time, where the effect of adding tin in 1:1 and 2:1 (Sn:Pt) atomic ratios to 0.63 wt. % Pt (Figures 6a and 6b) and 1.10 wt. % Pt (Figures 6c and 6d) catalyst, was investigated. For both Pt loadings, the addition of tin significantly enhanced selectivity toward ethylene beyond 90%, as well as markedly decreased the extent of catalyst deactivation (Liwu et al., 1990; de Miguel et al., 1996). For the Pt/γ-Al_2O_3 catalysts, without the addition of tin, ethylene selectivities near

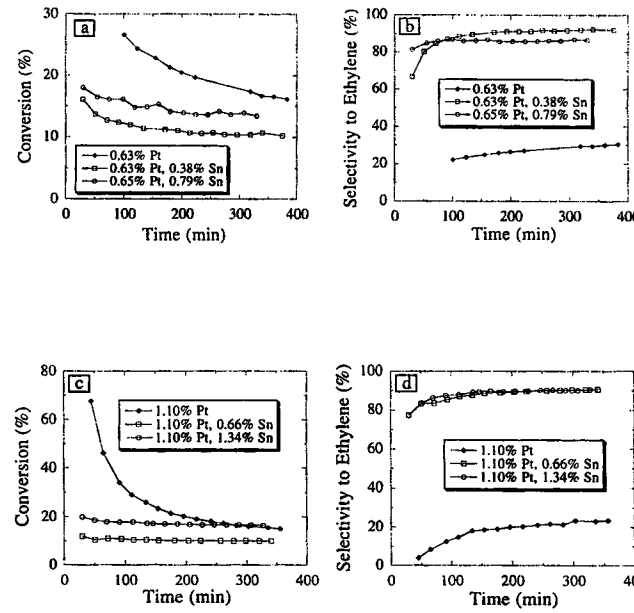

Figure 6. Catalyst selection results from FBR experiments with narrow surface-step platinum and uniform tin distributions.

0.63 wt. % Pt, 0.63 wt. % Pt with 0.38 wt. % Sn (1:1 Sn:Pt atomic ratio), and 0.65 wt. % Pt with 0.79 wt. % Sn (2:1 Sn:Pt atomic ratio). (a) Total conversion vs. time on stream, and (b) selectivity vs. time on stream; also the FBR results for catalysts containing 1.10 wt. % Pt, 1.10 wt. % Pt with 0.66 wt. % Sn (1:1 Sn:Pt atomic ratio), and 1.10 wt. % Pt with 1.34 wt. % Sn (2:1 Sn:Pt atomic ratio): (c) conversion vs. time on stream, and (d) selectivity vs. time on stream.

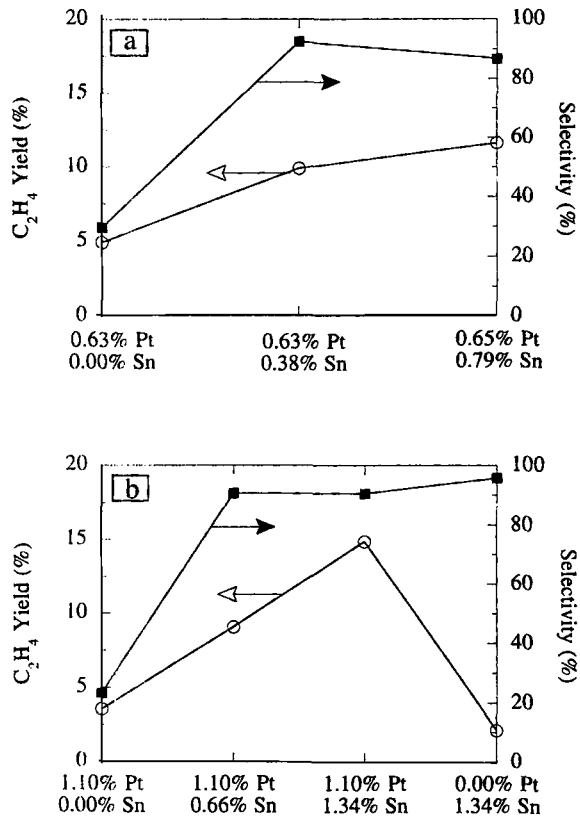

Figure 7. C_2H_4 yield and selectivity after 6 h on stream.

(a) 0.63 wt. % Pt, 0.63 wt. % Pt with 0.38 wt. % Sn (1:1 Sn:Pt atomic ratio), and 0.65 wt. % Pt with 0.79 wt. % Sn (2:1 Sn:Pt atomic ratio), and (b) 1.10 wt. % Pt, 1.10 wt. % with 0.66 wt. % Sn (1:1 Sn:Pt atomic ratio), and 1.10 wt. % Pt with 1.34 wt. % Sn (2:1 Sn:Pt atomic ratio).

20% and rapid deactivation due to coking were observed. For these catalysts, the predominant reaction was the hydrogenolysis of ethane to form methane (Sinfelt, 1984; Goddard et al., 1989).

Figures 7a and 7b show a summary of the different catalyst formulations after 6 h of operation. When comparing the two figures, it can be seen that the catalyst containing 1.10 wt. % Pt with 1.34 wt. % Sn, in a Sn:Pt atomic ratio of 2:1, resulted in the highest yield of 15.0% with a selectivity of 90.3%. The other bimetallic Pt/Sn catalysts also showed selectivities of 90% and higher; however, their dehydrogenation activities were considerably lower. The γ-Al_2O_3 support and the Sn/γ-Al_2O_3 catalyst were also tested for catalytic activity, and were found to be inactive and slightly active (~ 2.5% conversion), respectively.

Catalyst distribution

Based on the results of the previous section, the catalyst composition selected for further studies was 1.10 wt. % Pt and 1.34 wt. % Sn supported on γ-Al_2O_3 pellets, which was maintained fixed for the various platinum distributions shown in Figures 2a to 2d. In these figure the platinum distributions, after the reduction step, are clearly seen as dark bands with the active layer locations and thicknesses shown in Table 1. In all cases, tin was distributed uniformly within the pellets. This was confirmed by EDXS analysis, where a 120-μm

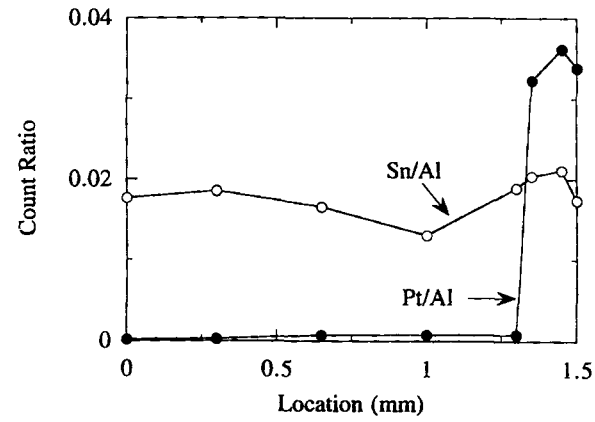

Figure 8. EDXS measurements of the Sn/Al and Pt/Al count ratios, at different radial positions within the narrow surface-step platinum catalyst pellet with 1.10 wt. % Pt and 1.34 wt. % Sn.

$\times$120-μm area was scanned at different radial positions within the 3-mm γ-Al_2O_3 support. Figure 8 shows the results of the EDXS scans, indicated as Sn/Al and Pt/Al count ratios, on a pellet with a narrow surface-step platinum distribution. It is clearly seen that tin is relatively uniform throughout the support, while platinum, as observed in Figure 2a, is concentrated near the surface of the pellet.

Catalyst characterization

Although the overall platinum loading was fixed at 1.10 wt. %, local platinum loadings within the steps varied from 2.7 wt. % (wide surface-step) to 11.1 wt. % (narrow subsurface-step). To evaluate the effect of platinum loading on the accessible platinum atoms and dispersion, hydrogen chemisorption experiments were conducted using γ-Al_2O_3 powders impregnated with platinum ranging from 0.1 wt. % to 6.5 wt. %. In Figure 9a, we can see that up to a loading of ~ 3.0 wt. % Pt, there is an approximately linear increase in surface platinum atoms, with dispersions in the range of 60% to 80% (Figure 9b). For higher loadings, the accessible platinum atoms remain essentially constant, with gradually decreasing dispersions to near 30%. A similar trend was observed by Dorling et al. (1970) for the Pt/SiO_2 system (see also Baratti et al., 1993). In Figure 9a, Eq. 7 was used to represent the experimental data up to 3.5 wt. % Pt loading, where the values for parts 9a and 9b were 2.14×10^2 m^2/(g Pt) and 12.8 g-catal/(g Pt), respectively. For loadings beyond 3.5 wt. % Pt, the Pt surface area was kept at a constant value of 4.8 m^2/(g-catal).

Since the distribution of Sn was essentially uniform and the overall Sn:Pt atomic ratio was maintained fixed at 2:1, the Sn:Pt ratios within the steps varied between 0.2:1 (narrow surface-step) and 0.5:1 (wide surface-step). Hydrogen chemisorption experiments were conducted on a 1.17 wt. % Pt/γ-Al_2O_3 catalyst powder for varying Sn:Pt atomic ratios (Merlen et al., 1996). As seen in Figures 10a and 10b, adding tin up to 1.36 wt. % resulted in no significant change in the accessible platinum atoms or dispersion (~ 80%).

The results of the hydrogen chemisorption measurements are shown in Table 1. The pellets were crushed to powder

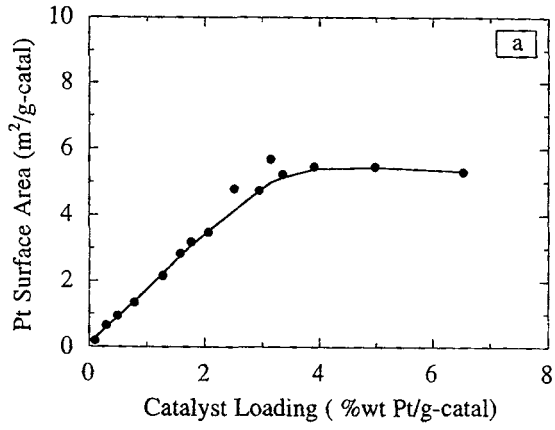

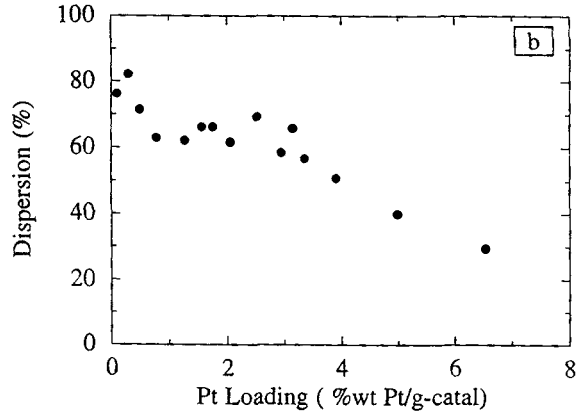

Figure 9. Effect of platinum loading, deposited on powdered γ-alumina support, on (a) platinum surface area, and (b) the platinum dispersion.

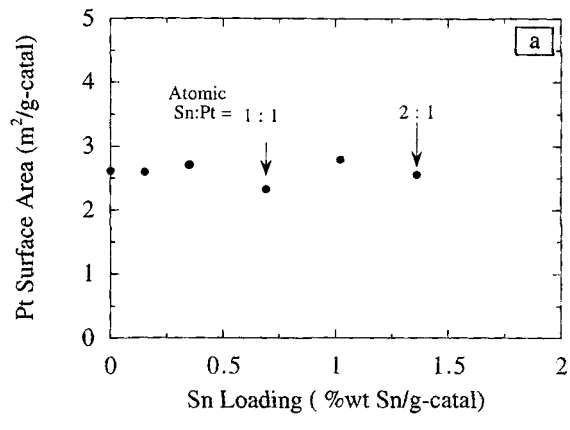

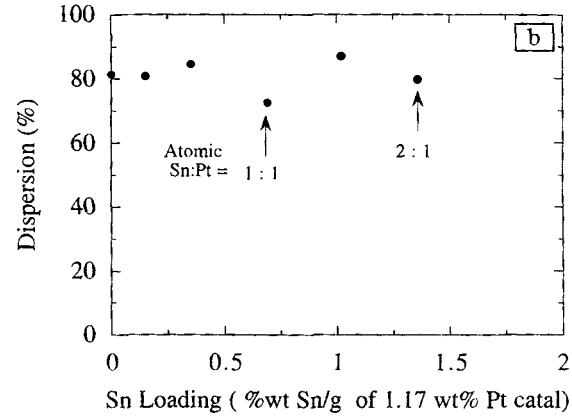

Figure 10. Effect of tin loading, impregnated on 1.17 wt. % Pt/γ-Al_2O_3 powder, on (a) the accessible platinum surface area, and (b) the platinum dispersion.

prior to measurements, and the resulting dispersions were in the range of ~35% (deep subsurface-step) to ~65% (narrow surface-step). As discussed earlier, addition of tin did not significantly alter platinum dispersion.

Intrinsic kinetics

To minimize intraparticle diffusional resistance, intrinsic kinetic experiments were conducted on catalyst powder with 1.10 wt. % Pt and 1.36 wt. % Sn supported on γ-Al_2O_3. The following rate expression was used to fit the data for ethane dehydrogenation (Champagnie et al., 1992; Gobina et al., 1995):

$$R(p_i) = k\left[p_{C_2H_6} - \frac{p_{C_2H_4}p_{H_2}}{K_{eq}}\right]. \tag{18}$$

The kinetic rate constant, k, is given by

$$k = k_0 \exp\left[-\frac{E}{R_G T}\right], \tag{19}$$

where $k_0 = 4.23\times10^{-3}$ mol/(cm^2·atm·s) and the activation energy (E = 18.2 kcal/mol) were found to fit the rate data. The E value was comparable to 20.6 and 18.1 kcal/mol reported by Champagnie et al. (1992) and Gobina et al. (1995), respectively.

Packed-bed membrane reactor

For the PBMR studies, the effects of nonuniform catalyst distribution involving various widths and catalyst locations were investigated both experimentally and theoretically. In these experiments, the comparisons were made by maintaining a constant overall metal loading. Experiments were also conducted to evaluate the effects of membrane thickness, feed composition, and sweep ratio. For all the PBMR and FBR experiments, the dehydrogenation selectivity toward ethylene was always greater than 95% (generally 98–99%), with carbon balances closing typically to within 2%, without ever exceeding 5%.

The Effects of Nonuniform Catalyst Distribution. The effects of residence time and temperature on reactor conversion are shown for varying active layer widths (Figures 11a and 11b) and platinum step locations (Figures 12a and 12b).

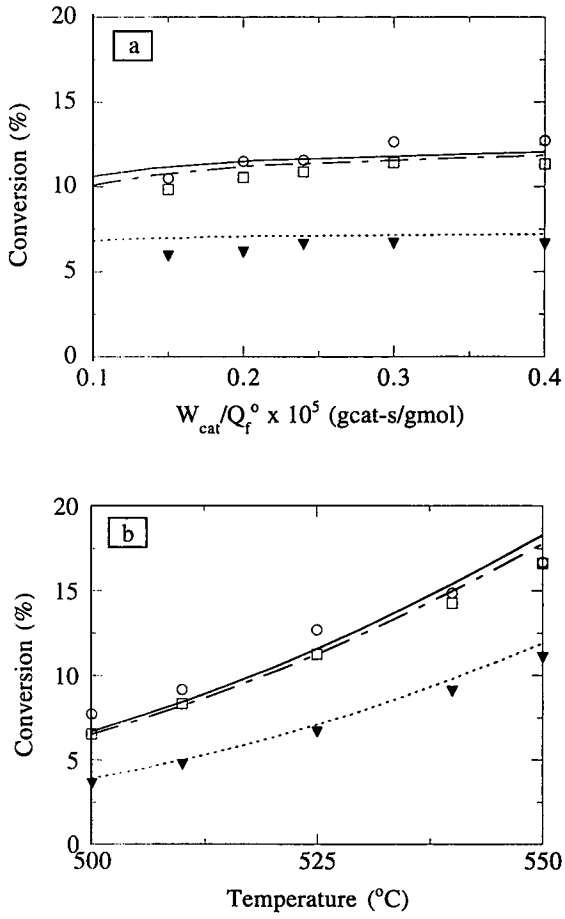

Figure 11. Effect of (a) residence time, W_{cat}/Q_f°, and (b) temperature on the conversion of ethane, in a PBMR and FBR, for the narrow surface-step and wide surface-step platinum distributions.

The symbols and lines are the experimental data and the model results, respectively. ○ and ——: narrow surface-step; □ and — — —: wide surface-step; ▾ and ------: fixed-bed reactor with narrow surface-step.

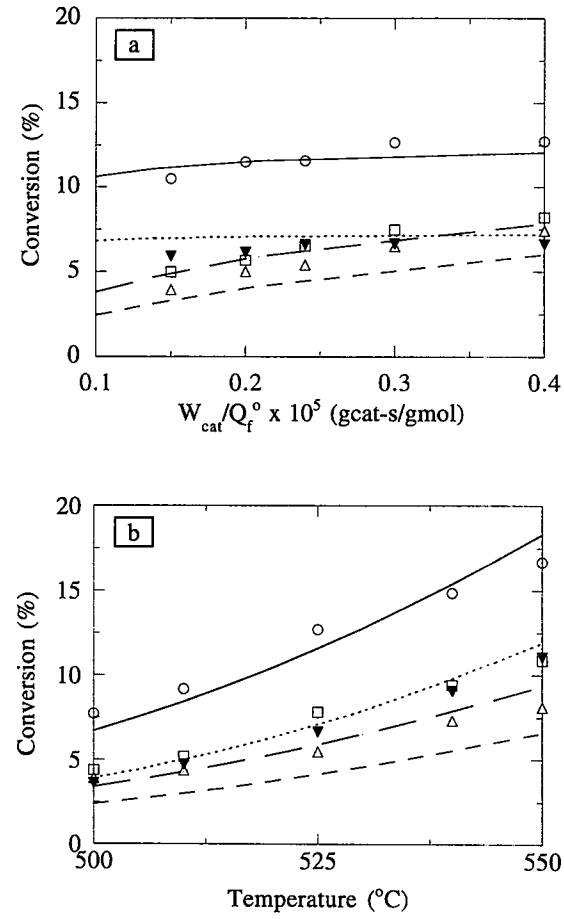

Figure 12. Effect of (a) residence time, W_{cat}/Q_f°, and (b) temperature on the conversion of ethane, in a PBMR and FBR, for the narrow surface-step, near surface-step, and deep subsurface-step platinum distributions.

The symbols and lines are the experimental data and the model results, respectively. ○ and ——: narrow surface-step; □ and — —: near surface-step; △ and – – –: deep subsurface-step; ▾ and -----: fixed-bed reactor with narrow surface-step.

The results of numerical calculations, using Eqs. 11–19, are also shown in these figures, where the effect of varying active surface areas as a function of different catalyst distributions is accounted for by incorporating Eq. 7 into the model (see Eq. 12). The experimental and calculated FBR results using the narrow surface-step catalyst are also included for comparison. The FBR conversions were within 5% of the equilibrium values, calculated based on the fresh feed introduced on the tube side of the membrane.

In Figure 11, both the narrow and wide surface-step catalysts exhibit conversions that exceed the FBR performance by nearly 80%. Also, the narrow surface-step catalysts yield conversions that are only slightly higher than for the wide surface-step. The relative closeness of results for the two cases can be explained by examining the values of the Thiele modulus, ϕ_p, which vary from 10.2 to 14.9 in the operating temperature range of 500°C to 550°C. These values indicate high reaction rates and consequent strong intrapellet diffusional resistance, so that the two surface-step distributions yield essentially the same reactor performance.

In Figure 12, the narrow surface-step catalyst is compared, both experimentally and numerically, to the near surface-step and the deep subsurface-step platinum distributions. By comparing Figures 11 and 12, we can see that the ethane conversion values are more significantly influenced by the active-layer location, than by the thickness near the surface. In fact, the performance of the subsurface catalyst in a PBMR is inferior to that for the narrow surface-step catalyst in a FBR. The decrease in reactor performance arises as a result of the strong diffusional resistance in the inert region, before the reactant contacts the active sites within the catalyst pellets. Since dehydrogenation of ethane is a positive-order reaction, where the rate increases with increasing reactant concentration, decreasing reaction rates are obtained as a consequence of the reactant concentration gradient. By placing the active layer as a narrow-step near the pellet surface, intrapellet diffusion limitations are minimized leading to a higher reaction rate.

It is worth noting that the numerical results in Figures 11

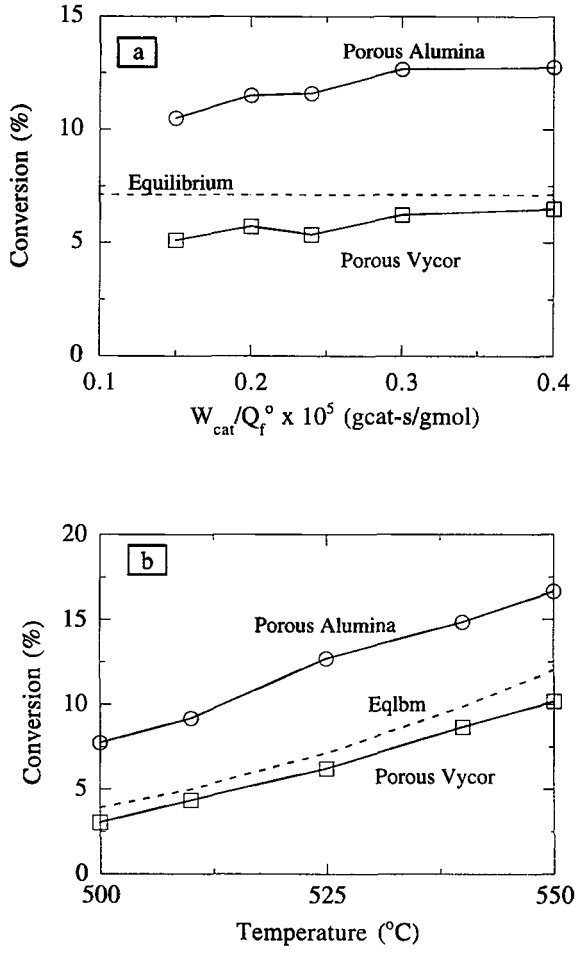

Figure 13. Effect of (a) residence time, W_{cat}/Q_f^o, and (b) temperature on the conversion of ethane, for the slip-cast modified alumina and porous Vycor membranes, using the narrow surface-step platinum catalyst.

and 12 were obtained without the use of *any* adjustable parameters. Using the intrinsic reaction kinetics and diffusion coefficients determined from separate experiments, the model yielded good agreement with experimental data in most cases. The slightly lower predictions for the two subsurface distributions arise because of residual platinum present in the outer largely inert region (see also Figures 2c and 2d).

Effect of Membrane Thickness. The effect of membrane thickness on reactor performance was examined by comparing the slip-cast-modified composite alumina (~ 17 μm thick) and porous Vycor (~ 1.2 mm thick) membranes (Figure 13). The catalyst with the narrow surface-step distribution was used for these experiments. The catalytic activity of both alumina and porous Vycor membranes was examined at reaction conditions up to a temperature of 550°C, and both membranes were found to be inert. Although not shown in Figure 13, the reaction experiments were also attempted using the original Membralox membrane (~ 2 μm thickness). Due to high permeation rates, however, the pressure conditions could not be sustained at the residence times investigated. Also, as a consequence of high permeation flux, significant reactant loss resulted in insufficient contact of the reactant gas with catalyst pellets, yielding subequilibrium conversion values.

As the membrane thickness is increased, the rate of reactant loss decreases, resulting in higher catalyst contact times. Further increase in membrane thickness, however, may decrease permeation rates to the extent that the effect of hydrogen separation on conversion enhancement is lost. Thus, upon addition of the ~ 15-μm γ-alumina layer to the original Membralox membrane, the reactant loss was significantly reduced, resulting in a higher catalyst contact time. However, the flux was still sufficiently high to result in effective hydrogen separation effect, to enhance reactor conversions to about 80% beyond the corresponding equilibrium values (see Figure 13). For the porous Vycor, the permeation thickness was ~ 1.2 mm, and as a result gas permeation rates were much lower as compared to the ~ 17-μm alumina membrane (measured to be ~ 170 times smaller). As a consequence of the low gas-permeation rates, the porous Vycor PBMR behaved essentially as a FBR (see Figure 13).

Effect of Feed Composition and Sweep Ratio. In Figure 14, the effect of residence time is studied for different feed compositions. As the ethane fraction in the feed increases, the overall conversion as well as the equilibrium conversion values decrease. Since the number of active sites is fixed, an increase in ethane concentration decreases the ratio of active sites to reactants, leading to a smaller reactant fraction converted to products.

For a constant feed flow rate, the effect of varying the argon sweep gas flow rate on the permeate side is shown in Figure 15. As the sweep ratio is increased, ethane conversion increases. This is expected because as argon flow increases, hydrogen is swept away at a faster rate, resulting in a larger hydrogen concentration gradient between the feed and permeate sides of the membrane. This results in increased hydrogen flux, leading to higher conversion enhancements.

Concluding Remarks

In this study, using dehydrogenation of ethane as an example, we have shown that improvements in PBMR performance can be obtained by proper catalyst design. A math-

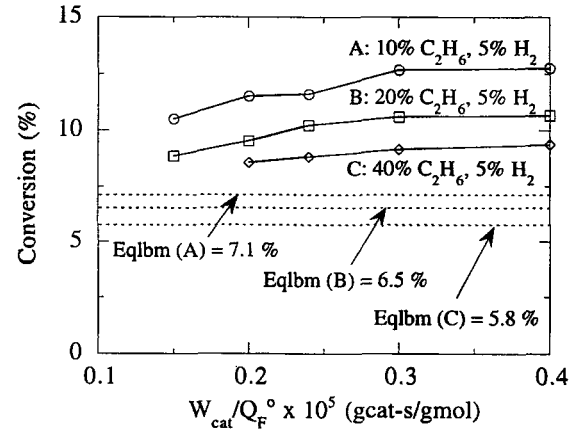

Figure 14. Effect of residence time, W_{cat}/Q_f^o on the conversion of ethane in the PBMR for varying feed concentrations, using the narrow surface-step platinum catalyst.

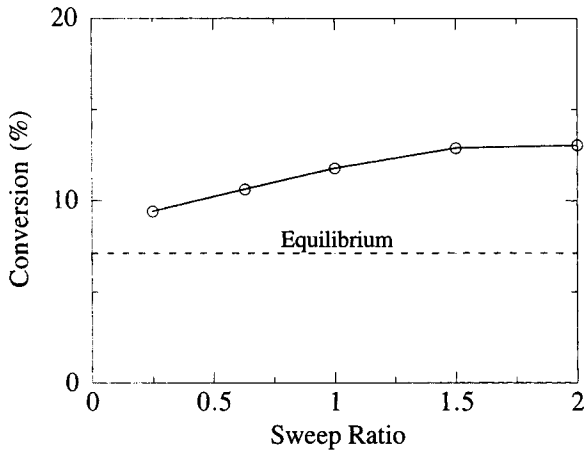

Figure 15. Effect of sweep ratio, β_p^o, on the conversion of ethane in the PBMR, using the narrow surface-step platinum catalyst.

ematical model was developed to examine the effect of nonuniform catalyst distributions. With the intrinsic reaction kinetics and diffusivities determined from separate experiments, the results of the model were found to be in good agreement with the experiments. The effect of membrane permeation on PBMR performance was also evaluated, using membranes with similar pore size but different thicknesses.

Bimetallic Pt-Sn/γ-Al_2O_3 catalyst, containing 1.10 wt. % Pt with 1.36 wt. % Sn was found to yield the highest activity, selectivity, and stability toward the dehydrogenation of ethane to ethylene. While maintaining a spatially uniform tin profile, catalysts with nonuniform platinum distributions were prepared for constant Pt and Sn loadings. For this positive-order isothermal reaction, it was shown that optimum PBMR performance is obtained when intrapellet mass-transfer resistance is minimized by concentrating the active layer as a narrow surface-step. Using such catalyst distributions, conversions nearly 80% above FBR values were obtained. Since the reactor model has been tested successfully in the present work, it can be utilized confidently to evaluate, and hence optimize, catalyst distributions for other cases involving arbitrary reaction kinetics.

The effect of membrane permeation on PBMR performance was also examined by comparing the original alumina ($\sim$ 2-μm membrane thickness), slip-cast-modified alumina ($\sim$ 17-μm membrane thickness), and the porous Vycor ($\sim$ 1.2-mm membrane thickness) membranes. For small thickness ($\sim$ 2 μm), the loss of reactant due to high permeation rate results in insufficient contact with the catalyst, leading to poor reactor performance. At the other extreme, for thick membranes (Vycor) the permeation rate is so low that the effect of hydrogen separation does not enhance reactor performance. Hence, the membrane thickness should be chosen such that the reactant loss is minimized, while maintaining a sufficiently high flux of the reaction components, to take full advantage of the enhancement gained by the separation effect of the membrane.

Acknowledgments

We gratefully acknowledge financial support from the National Science Foundation (grants CTS-9213683 and CTS-9529172). We also thank Vista Chemical Company for the alumina sol, and Engelhard Corporation for the γ-alumina support, both supplied free of charge. The AUTOSORB-1 apparatus for BET measurements was purchased by NSF Research Equipment Grant CTS-9412018.

Notation

b = constant in Eq. 7, g (catalyst support)/g (active component)
D_i = diffusivity of the ith component, cm^2/s
K_e = equilibrium constant, atm
K_{eq} = dimensionless equilibrium constant, K_e/P_{tube}
L = membrane length, cm
MW_i = molecular weight of component i
p_i = partial pressure of the ith component, atm
P = total pressure, atm
P_r = ratio of permeate to feed-side pressure, $P_{\text{perm}}/P_{\text{tube}}$
Q = molar flow rate, mol/s
r = radial position, cm
r_{pore} = membrane or pellet pore radius, cm
R = radius, cm
R_G = universal gas constant
s = dimensionless membrane radius
T = operating temperature, K
u_i = dimensionless partial pressure of the ith component in the membrane
V_p = pellet volume, cm^3
V_{cat} = catalyst volume, cm^3
w = dimensionless pellet radius
W_{cat} = weight of catalyst pellets, g
α = diffusivity ratio
β_{perm}^o = sweep ratio
Δ = width of step distribution
ϵ = void fraction on the feed side of PBMR
φ = dimensionless space time within the packed bed
θ = dimensionless space time within membrane
ψ_i = dimensionless partial pressure of the ith component in the pellets

Subscripts and superscript

c = center of step distribution
cat = catalyst
m = membrane
p = pellet
o = inlet conditions

Literature Cited

Baratti, R., H. Wu, M. Morbidelli, and A. Varma, "Optimal Catalyst Activity Profiles in Pellets-X. The Role of Catalyst Loading," *Chem. Eng. Sci.*, **48**, 1869 (1993).

Beltramini, J., and D. L. Trimm, "Activity, Selectivity and Coking Over Mono- and Bi-metallic Reforming Catalysts," *Appl. Catal.*, **32**, 71 (1987).

Bernstein, L. A., and C. R. F. Lund, "Membrane Reactors for Catalytic Series and Series-parallel Reactions," *J. Memb. Sci.*, **77**, 155 (1993).

Cannon, K. C., and J. J. Hacskaylo, "Evaluation of Palladium-Impregnation on the Performance of a Vycor Glass Catalytic Membrane Reactor," *J. Memb. Sci.*, **65**, 259 (1992).

Cavani, F., and F. Trifiro, "Skillful Matching of Chemistry and Engineering in Catalytic Dehydrogenation of Low-Molecular-Weight Paraffins," *Chim. Ind. (Milan)*, **76**(11), 708 (1994).

Champagnie, A. M., T. T. Tsotsis, R. G. Minet, and E. Wagner, "The Study of Ethane Dehydrogenation in a Catalytic Membrane Reactor," *J. Catal.*, **134**, 713 (1992).

Cortright, R. D., and J. A. Dumesic, "Microcalorimetric, Spectroscopic, and Kinetic Studies of Silica-Supported Pt and Pt/Sn Catalysts for Isobutane Dehydrogenation," *J. Catal.*, **148**, 771 (1994).

de Miguel, S., A. Castro, and O. Scelza, "FTIR and XPS Study of Supported PtSn Catalysts Used for Light Paraffins Dehydrogenation," *Catal. Lett.*, **36**, 201 (1996).

Dorling, T. A., B. W. J. Lynch, and R. L. Moss, "The Structure and Activity of Supported Metal Catalysts V. Variables in the Preparation of Platinum/Silica Catalysts," *J. Catal.*, **20**, 190 (1970).

Finlayson, B. A., *Nonlinear Analysis in Chemical Engineering*, McGraw Hill, New York (1980).
Freel, J., "Chemisorption on Supported Platinum I. Evaluation of a Pulse Method," *J. Catal.*, **25**, 139 (1972).
Gavriilidis, A., A. Varma, and M. Morbidelli, "Optimal Distribution of Catalyst in Pellets," *Catal. Rev.—Sci. Eng.*, **35**, 399 (1993).
Gobina, E., K. Hou, and R. Hughes, "Ethane Dehydrogenation in a Catalytic Membrane Reactor Coupled with a Reactive Sweep Gas," *Chem. Eng. Sci.*, **50**, 2311 (1995).
Goddard, S. A., M. D. Amiridis, J. E. Rekoske, N. Cardona-Martinez, and J. A. Dumesic, "Kinetic Simulation of Heterogeneous Catalytic Processes: Ethane Hydrogenolysis Over Supported Group VIII Metals," *J. Catal.*, **117**, 155 (1989).
Hsieh, H. P., "Inorganic Membrane Reactors," *Catal. Rev.—Sci. Eng.*, **33**, 1 (1991).
Huang, Z., J. R. Fryer, C. Park, D. Stirling, and G. Webb, "Transmission Electron Microscopy and Energy Dispersive X-Ray Spectroscopy Studies of Pt-Sn/γ-Al_2O_3 Catalysts," *J. Catal.*, **159**, 340 (1996).
IMSL Inc., *Fortran Subroutines for Mathematical Applications*, IMSL Math Library, Houston (1989).
Ito, N., Y. Shindo, K. Haraya, K. Obata, T. Hakuta, and H. Yoshitome, "Simulation of a Reaction Accompanied by Separation," *Int. Chem. Eng.*, **25**, 138 (1985).
Lee, S.-Y., and R. Aris, "The Distribution of Active Ingredients in Supported Catalysts Prepared by Impregnation," *Catal. Rev.—Sci. Eng.*, **27**, 207 (1985).
Liwu, L., Z. Tao, Z. Jingling, and X. Zhusheng, "Dynamic Process of Carbon Deposition on Pt and Pt-Sn Catalysts for Alkane Dehydrogenation," *Appl. Catal.*, **67**, 11 (1990).
Merlen, E., P. Beccat, J. C. Bertolini, P. Delichere, N. Zanier, and B. Didillon, "Characterization of Bimetallic Pt-Sn/Al_2O_3 Catalysts: Relationship Between Particle Size and Structure," *J. Catal.*, **159**, 178 (1996).
Mohan, K., and R. Govind, "Analysis of Equilibrium Shift in Isothermal Reactors with a Permselective Wall," *AIChE J.*, **34**, 1493 (1988).
Papageorgiou, P., D. M. Price, A. Gavriilidis, and A. Varma, "Preparation of Pt/γ-Al_2O_3 Pellets with Internal Step-Distribution of Catalyst: Experimental and Theory," *J. Catal.*, **158**, 439 (1996).
Raich, B. A., and H. C. Foley, "Supra-equilibrium Conversion in Palladium Membrane Reactors: Kinetic Sensitivity and Time Dependence," *Appl. Catal. A. Gen.*, **129**, 167 (1995).
Santos, A., J. Coronas, M. Menendez, and J. Santamaria, "Catalytic Partial Oxidation of Methane to Synthesis Gas in a Ceramic Membrane Reactor," *Catal. Lett.*, **30**, 189 (1995).
Saracco, G., and V. Speccia, "Catalytic Inorganic-Membrane Reactors: Present Experience and Future Opportunities," *Catal. Rev.—Sci. Eng.*, **36**, 305 (1994).
Sarkany, J., and R. D. Gonzalez, "On the Use of the Dynamic Pulse Method to Measure Metal Surface Areas," *J. Catal.*, **76**, 75 (1982).
Sinfelt, J. H., *Bimetallic Catalysts*, Wiley, New York (1983).
Sun, Y.-M., and S.-J. Khang, "Catalytic Membrane for Simultaneous Chemical Reaction and Separation Applied to Dehydrogenation Reaction," *Ind. Eng. Chem. Res.*, **27**, 1136 (1988).
Tonkovich, A. L. Y., J. L. Zilka, D. M. Jiminez, G. L. Roberts, and J. L. Cox, "Experimental Investigations of Inorganic Membrane Reactors: A Distributed Feed Approach for Partial Oxidation Reactions," *Chem. Eng. Sci.*, **51**, 789 (1996).
Tsotsis, T. T., A. M. Champagnie, R. G. Minet, and P. K. T. Liu, "Catalytic Membrane Reactors," *Computer Aided Design of Catalysts*, Chap. 12, E. R. Becker and C. J. Pereira, eds., Dekker, New York (1993).
Uhlhorn, R. J. R., M. H. B. J. Huis In't Veld, K. Keizer, and A. J. Burggraaf, "Synthesis of Ceramic Membranes: Part I Synthesis of Non-supported and Supported γ-Alumina Membranes Without Defects," *J. Mater. Sci.*, **27**, 527 (1992).
Villadsen, J., and M. L. Michelsen, *Solution of Differential Equation Models by Polynomial Approximation*, Prentice Hall, Englewood Cliffs, NJ (1978).
Ward, D. A., and E. I. Ko, "Preparing Catalytic Materials by the Sol-Gel Method," *Ind. Eng. Chem. Res.*, **34**, 421 (1995).
Yeung, K. L., R. Aravind, J. Szegner, and A. Varma, "Metal Composite Membranes: Synthesis, Characterization and Reaction Studies," *Stud. Surf. Sci. Catal.*, **101**, 1349 (1996).
Yeung, K. L., R. Aravind, R. J. X. Zawada, J. Szegner, G. Cao, and A. Varma, "Nonuniform Catalyst Distribution for Inorganic Membrane Reactors: Theoretical Considerations and Preparation Techniques," *Chem. Eng. Sci.*, **49**, 4823 (1994).
Yeung, K. L., J. M. Sebastian, and A. Varma, "Mesoporous Alumina Membranes: Synthesis, Characterization, Thermal Stability and Nonuniform Distribution of Catalyst," *J. Memb. Sci.*, **131**, 9 (1997).
Zaman, J., and A. Chakma, "Inorganic Membrane Reactors," *J. Memb. Sci.*, **92**, 1 (1994).
Zaspalis, V. T., W. van Praag, K. Keizer, J. G. van Ommen, J. R. H. Ross, and A. J. Burggraaf, "Reactor Studies Using Alumina Separation Membranes for the Dehydrogenation of Methanol and n-Butane," *Appl. Catal.*, **74**, 223 (1991).
Ziaka, Z. D., R. G. Minet, and T. T. Tsotsis, "A High Temperature Catalytic Membrane Reactor for Propane Dehydrogenation," *J. Memb. Sci.*, **93**, 221 (1993).

Manuscript received Dec. 2, 1996, and revision received Mar. 3, 1997.